Supplementary Information

Multi-responsive actuators based on a graphene oxide composite: intelligent robot and bioinspired applications

Luzhuo Chen,*‡[a, b] Mingcen Weng,‡[a, b] Peidi Zhou,[a, b] Lingling Zhang,[a, b] Zhigao Huang[a, b] and Wei Zhang*[a, b]

[a]Fujian Provincial Key Laboratory of Quantum Manipulation and New Energy Materials, College of Physics and Energy, Fujian Normal University, Fuzhou 350117, China

E-mail: chenluzhuo@163.com, wzhang721@163.com

[b]Fujian Provincial Collaborative Innovation Center for Optoelectronic Semiconductors and Efficient Devices, Xiamen 361005, China

‡These authors contributed equally.

Supplementary Notes

Supplementary Note S1: Bending curvature calculation principle of the GO/BOPP actuator

The calculation principle is the same as reported before.[1] The parameters are defined as follows (shown in Fig. S6):

L: The length of the GO/BOPP actuator.

ρ: The radius of the arc of curved GO/BOPP actuator.

x: The horizontal displacement of the curved GO/BOPP actuator.

y: The vertical displacement of the curved GO/BOPP actuator.

$\theta/2$: The chord tangent angle of the curved GO/BOPP actuator.

θ: The bending angle of the arc of the curved GO/BOPP actuator.

The curvature is defined as the reciprocal of radius ($1/\rho$).

The chord tangent angle is given by

$$\frac{\theta}{2} = \tan^{-1}\frac{x}{L-y} \tag{1}$$

As the bending angle is given by

$$\theta = \frac{L}{\rho} \tag{2}$$

the curvature $1/\rho$ is deduced as

$$\frac{1}{\rho} = \frac{\theta}{L}. \tag{3}$$

Hence, the curvature of the actuator can be calculated by using the bending angle and length of the actuator.

Supplementary Note S2: Theoretical model of the humidity-driven motion of GO/BOPP actuator

Similar to the deformation of bilayer actuators reported before,[2, 3] GO/BOPP bilayer actuator is approximated to be composed of GO layer (layer 1) and BOPP layer (layer 2). When the humidity decreases, the actuator bends towards GO side due to the water desorption of the GO paper. Since the actuator is bending, all forces acting over the cross-section of GO layer can be represented as an axial tensile force (P_1) and bending moment (M_1). On the other side, axial compressive force (P_2) and bending moment (M_2) are acting in the cross-section of BOPP layer. Because no external forces are acting on the actuator, all internal forces acting on cross-section of the bilayer structure should be in equilibrium. Hence,

$$P = P_1 = P_2, \tag{4}$$

$$\left(\frac{t_1+t_2}{2}\right) P = M_1 + M_2. \tag{5}$$

From the beam theory,

$$M_1 = \frac{E_1 I_1}{\rho},\ M_2 = \frac{E_2 I_2}{\rho},\ I_1 = \frac{b t_1^3}{12} \text{ and } I_2 = \frac{b t_2^3}{12} \tag{6}$$

where ρ is the radius of the curved GO/BOPP actuator, E_1 and E_2 are Young's modules of the GO layer and BOPP layer respectively, I_1 and I_2 are the moment of inertia for GO layer and BOPP layer, b is the width of the actuator, and t_1 and t_2 are the thickness of GO layer and BOPP layer, respectively. By substituting M_1 and M_2 into equation (5), we have:

$$\left(\frac{t_1+t_2}{2}\right) P = \frac{E_1 I_1}{\rho} + \frac{E_2 I_2}{\rho} \tag{7}$$

Because equation (7) has two unknown variables, another equation should be given. The normal strain is the same at the interface of GO layer and BOPP layer. Moreover, the normal strain is the sum of strains caused by the axial force (P), bending of the actuator, hygroscopic expansion of GO layer. Therefore, hygroexpansive strain can be expressed as:

$$\varepsilon_h = \beta \Delta C. \tag{8}$$

As the hygroexpansion of BOPP layer is negligible, we have,

$$\beta_1 \Delta C_1 + \frac{t_1}{2\rho} + \frac{P}{E_1 t_1 b} = -\frac{t_2}{2\rho} - \frac{P}{E_2 t_2 b} \tag{9}$$

where ε_h is hygroexpansive strain, β_1 is the CHE of GO layer and ΔC_1 is the change of moisture content in the GO layer. Then,

$$\frac{1}{2\rho}(t_1 + t_2) = -\beta_1 \Delta C_1 - \left(\frac{1}{E_1 t_1 b} + \frac{1}{E_2 t_2 b}\right) P \tag{10}$$

By substituting P value, we have:

$$\frac{1}{2\rho}(t_1 + t_2) = -\beta_1 \Delta C_1 - \frac{2}{\rho}\left(\frac{1}{E_1 t_1 b} + \frac{1}{E_2 t_2 b}\right)\left(\frac{E_1 I_1 + E_2 I_2}{t_1 + t_2}\right) \tag{11}$$

The curvature of the actuator can be calculated:

$$\frac{1}{\rho} = \frac{6E_1E_2t_1t_2(t_1+t_2)(-\beta_1\Delta C_1)}{\left(E_1t_1^2\right)^2+\left(E_2t_2^2\right)^2+2E_1E_2t_1t_2(2t_1^2+3t_1t_2+2t_2^2)} \tag{12}$$

We calculated the total curvature of the actuator by replacing ΔC_1 as follows:

$$\Delta C_1 = C_{RH} - C_{50\%} \tag{13}$$

Therefore,

$$\frac{1}{\rho} = \frac{6E_1E_2t_1t_2(t_1+t_2)(-\beta_1(C_{RH}-C_{50\%}))}{\left(E_1t_1^2\right)^2+\left(E_2t_2^2\right)^2+2E_1E_2t_1t_2(2t_1^2+3t_1t_2+2t_2^2)} \tag{14}$$

where β_1 is calculated according to previous report.[4] The length change of GO fiber is roughly 5% and the diameter change of GO fiber is 1.5% when the RH increases from 25% to 80%. Hence, the relationship between ε_h and RH can be obtained. Furthermore, from Fig. 2f, we have a liner fitting function:

$$C_{RH} = 0.538 \times RH \tag{15}$$

From equation (8), as the ε_h and moisture content change ΔC are given, the CHE β is calculated to be in the range of 0.05 ~ 0.16 C^{-1}. In our model, β_1 is set to be 0.12 C^{-1}. E_1= 32 GPa, E_2= 1.1 GPa, t_1= 30 μm, and t_2= 40 μm.

Supplementary Note S3: Theoretical model of the NIR light-driven motion of GO/BOPP actuator

When the GO/BOPP actuator is driven by NIR light, thermal expansion and hygroexpansion of GO layer are accompanied with thermal expansion of BOPP layer. Thus, hygroexpansive strain can be expressed as:

$$\varepsilon_h = \beta \Delta C \tag{16}$$

and thermal expansive strain can be expressed as:

$$\varepsilon_{thermal} = \alpha \Delta T \tag{17}$$

Therefore, similar to the deduction of Note S2 and the hygroexpansion of BOPP layer is negligible, we can have the following equation:

$$\alpha_1 \Delta T + \beta_1 \Delta C_1 + \frac{t_1}{2\rho} + \frac{P}{E_1 t_1 b} = \alpha_2 \Delta T - \frac{t_2}{2\rho} - \frac{P}{E_2 t_2 b} \tag{18}$$

where α_1 and α_2 are the CTE of the GO layer and BOPP layer respectively, ΔT is the temperature change, β_1 is the CHE of the GO layer, and ΔC_1 is the change of the moisture content in the GO layer.

Then,

$$\frac{1}{2\rho}(t_1 + t_2) = \alpha_2 \Delta T - \alpha_1 \Delta T - \beta_1 \Delta C_1 - \left(\frac{1}{E_1 t_1 b} + \frac{1}{E_2 t_2 b}\right) P \tag{19}$$

By adding P value:

$$\frac{1}{2\rho}(t_1 + t_2) = \alpha_2 \Delta T - \alpha_1 \Delta T - \beta_1 \Delta C_1 - \frac{2}{\rho}\left(\frac{1}{E_1 t_1 b} + \frac{1}{E_2 t_2 b}\right)\left(\frac{E_1 I_1 + E_2 I_2}{t_1 + t_2}\right) \tag{20}$$

The curvature of the actuator then can be calculated:

$$\frac{1}{\rho} = \frac{6E_1 E_2 t_1 t_2 (t_1 + t_2)(\alpha_2 \Delta T - \alpha_1 \Delta T - \beta_1 \Delta C_1)}{(E_1 t_1^2)^2 + (E_2 t_2^2)^2 + 2E_1 E_2 t_1 t_2 (2t_1^2 + 3t_1 t_2 + 2t_2^2)} \tag{21}$$

We calculated the total curvature of the actuator as a function of temperature by replacing ΔC_1 (Fig. S15):

$$C_T = -0.306 \times T + 30.79 \tag{22}$$

$$\Delta C_1 = -0.306 \times \Delta T + 30.79 \tag{23}$$

Therefore,

$$\frac{1}{\rho} = \frac{6E_1 E_2 t_1 t_2 (t_1 + t_2)(\alpha_2 \Delta T - \alpha_1 \Delta T - \beta_1 (-0.306 \times \Delta T + 30.79))}{(E_1 t_1^2)^2 + (E_2 t_2^2)^2 + 2E_1 E_2 t_1 t_2 (2t_1^2 + 3t_1 t_2 + 2t_2^2)} \tag{24}$$

where E_1= 32 GPa, E_2= 1.1 GPa, α_1= 0.85 ppm K^{-1}, β_1= 0.12 C^{-1}, α_2= 137 ppm K^{-1}, t_1= 30 μm, and t_2= 40 μm, respectively.

If we only consider thermal expansion of GO layer and BOPP layer, β_1 is set to be 0. Therefore, the theoretical curvature can be expressed as:

$$\frac{1}{\rho}=\frac{6E_1E_2t_1t_2(t_1+t_2)(\alpha_2\Delta T-\alpha_1\Delta T)}{(E_1t_1^2)^2+(E_2t_2^2)^2+2E_1E_2t_1t_2(2t_1^2+3t_1t_2+2t_2^2)} \tag{25}$$

The calculated results are shown in Fig. S15b with blue triangle.

If we only consider the thermohygration effect of GO layer, α_1 and α_2 are set to be 0, so the theoretical curvature can be expressed as:

$$\frac{1}{\rho}=\frac{6E_1E_2t_1t_2(t_1+t_2)(-\beta_1(-0.306\times\Delta T+30.79))}{(E_1t_1^2)^2+(E_2t_2^2)^2+2E_1E_2t_1t_2(2t_1^2+3t_1t_2+2t_2^2)} \tag{26}$$

The calculated results are shown in Fig. S15b with pink triangle.

Supplementary Note S4: Influence of GO paper thickness on the actuation performance

In this study, the thicknesses of GO layer in GO/BOPP actuators are all selected as 30 μm. We also studied the influence of the GO layer thickness on the actuation performance. First of all, we measured the curvatures of the GO/BOPP actuators with different GO layer thicknesses when they were driven by humidity. When the RH decreased from 50% to 20%, the curvature of the actuator with a GO layer thickness of 6.3 μm was about 0.86 cm^{-1} (Fig. S17a). With the thickness increase of the GO layer, the curvature initially increased to 2.8 cm^{-1} for the actuator with GO layer thickness of 35 μm, and then gradually decreased to 0.3 cm^{-1} as the GO layer thickness increased to 94 μm. Similarly, when the RH increased from 50% to 90%, the curvature of the actuator with a GO layer thickness of 6.3 μm was about 0.3 cm^{-1} (Fig. S17a). With the thickness increase of the GO layer, the curvature initially increased to 4.1 cm^{-1} for the actuator with a GO layer thickness of 44.3 μm, and then gradually decreased to 0.2 cm^{-1} as the GO layer thickness increased to 94 μm (Fig. S17a).

The influence of the GO layer thickness on light-driven actuation performance was studied as well. We measured the curvatures of the GO/BOPP actuators with different GO layer thicknesses when they were driven by NIR light. With NIR light power density of 300 mW cm^{-2}, the curvature of the actuator with a GO layer thickness of 6.3 μm was about 2.5 cm^{-1} (Fig. S17b). With the thickness increase of the GO layer, the curvature initially increased to 3.1 cm^{-1} for the actuator with a GO layer thickness of 25.5 μm, and then gradually decreased to 0.3 cm^{-1} as the GO layer thickness increased to 94 μm (Fig. S17b).

In a word, when the GO/BOPP actuators are driven by humidity, the optimal thickness of the GO layer to obtain a large curvature is in the range of 35 - 44.3 μm. When the actuators are driven by NIR light, the optimal thickness of the GO layer to obtain a large curvature is around 25.5 μm. To obtain a large bending curvature of the multi-responsive GO/BOPP actuator, the thickness of the GO layer should be neither too small, nor too large. Hence, it is appropriate to select the thickness of GO layer thickness as 30 μm (between 25.5 μm and 44.3 μm) in this study.

Supplementary Movies.

Movie S1: Twisting and untwisting actuations of the helical GO/BOPP actuator.

Movie S2: Grasping and releasing process of the robot arm.

Supplementary Figures

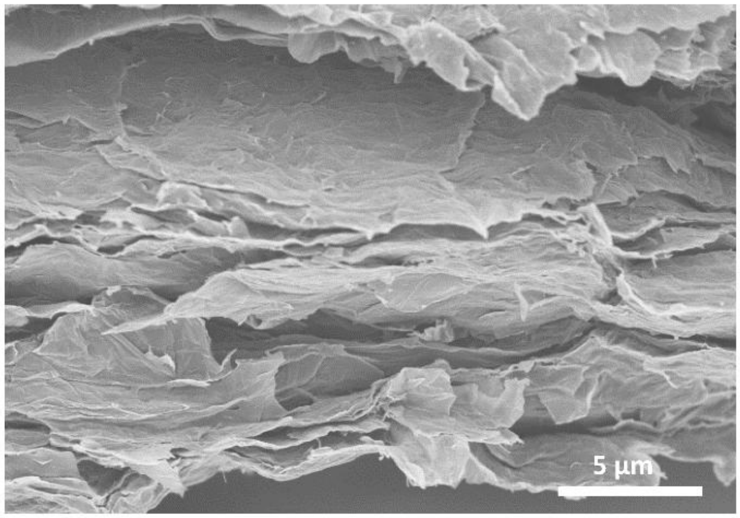

Fig. S1. Cross-sectional SEM image of GO paper.

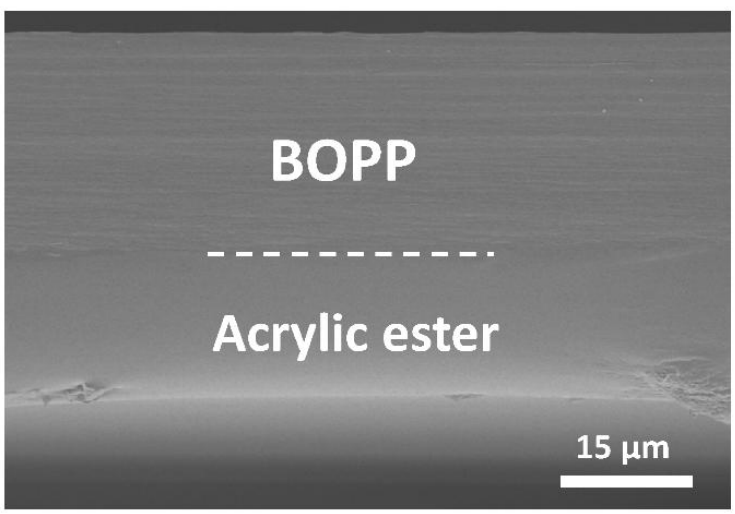

Fig. S2. Cross-sectional SEM image of BOPP film coated with acrylic ester.

Fig. S3. Optical photo showing the flexibility of the GO/BOPP actuator.

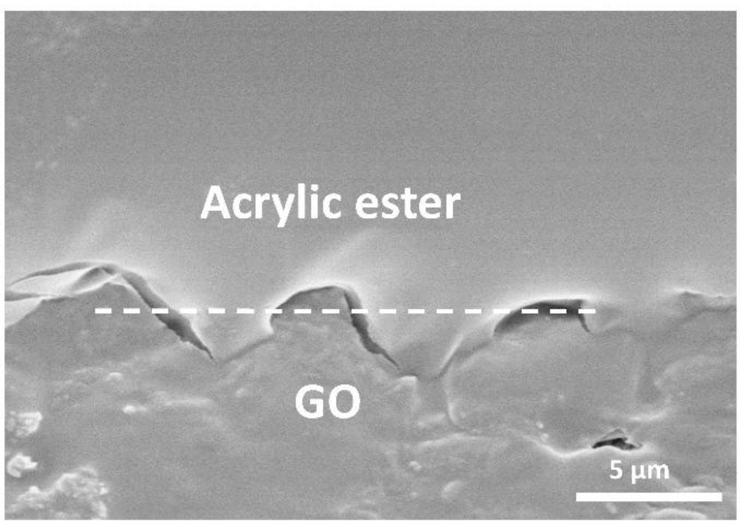

Fig. S4. Cross-sectional SEM image with higher magnification of the GO/BOPP actuator.

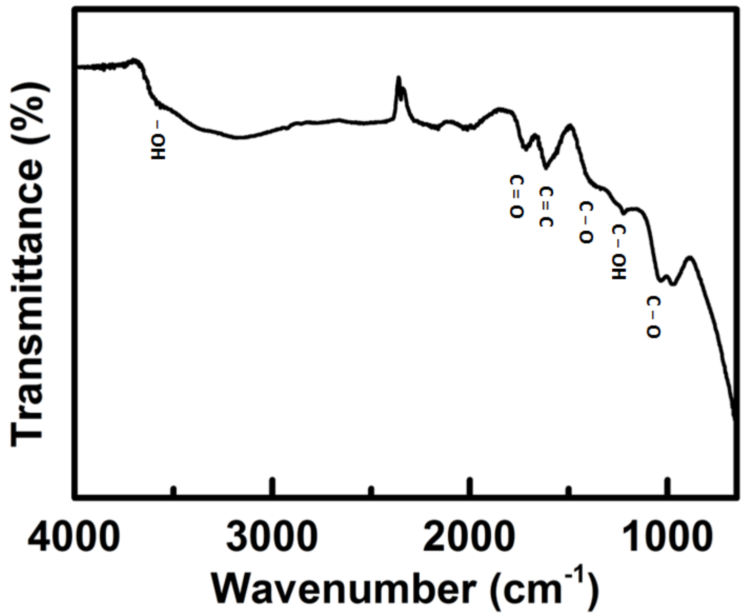

Fig. S5. FT-IR spectrum of GO paper.

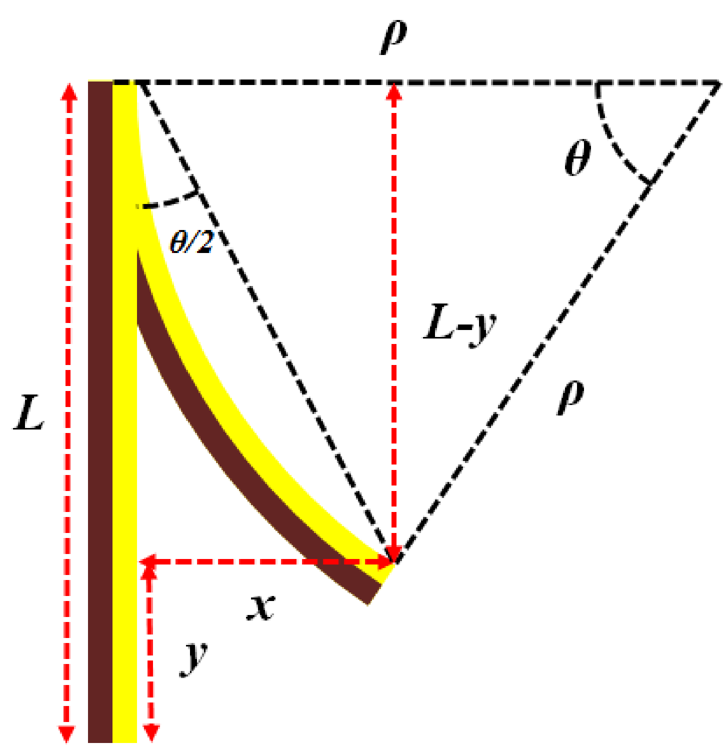

Fig. S6. The GO/BOPP actuator with correlative parameters for calculating the bending curvature.

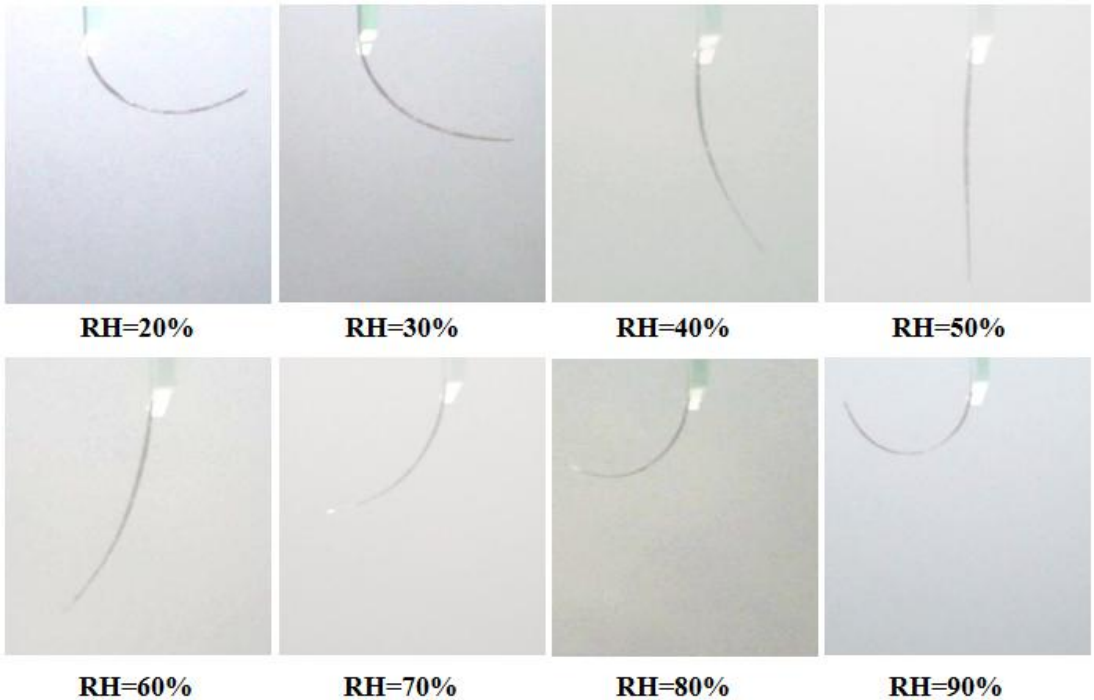

Fig. S7. Actuation of the GO/BOPP actuator at different RH.

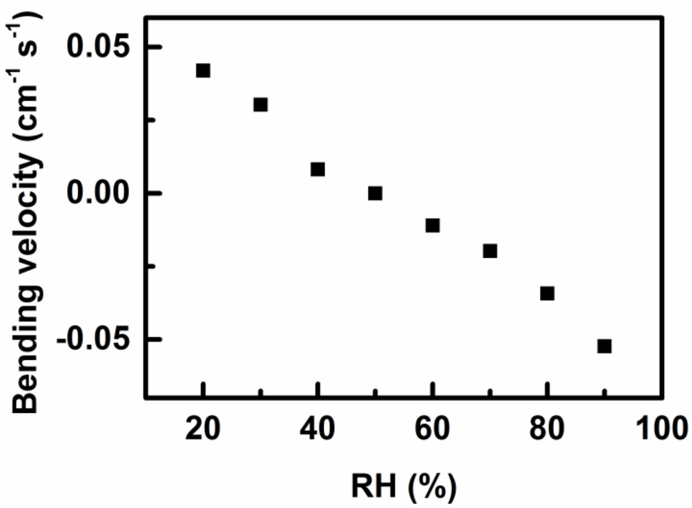

Fig. S8. Bending velocity of the GO/BOPP actuator as a function of RH. The dimensions of the actuators are 15 mm × 2 mm × 65 μm (length × width × thickness).

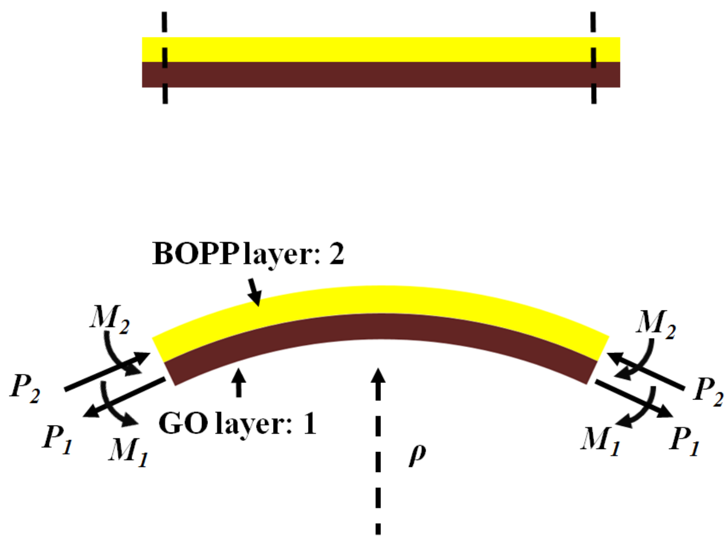

Fig. S9. Schematic illustration of the GO/BOPP bilayer actuator for modeling.

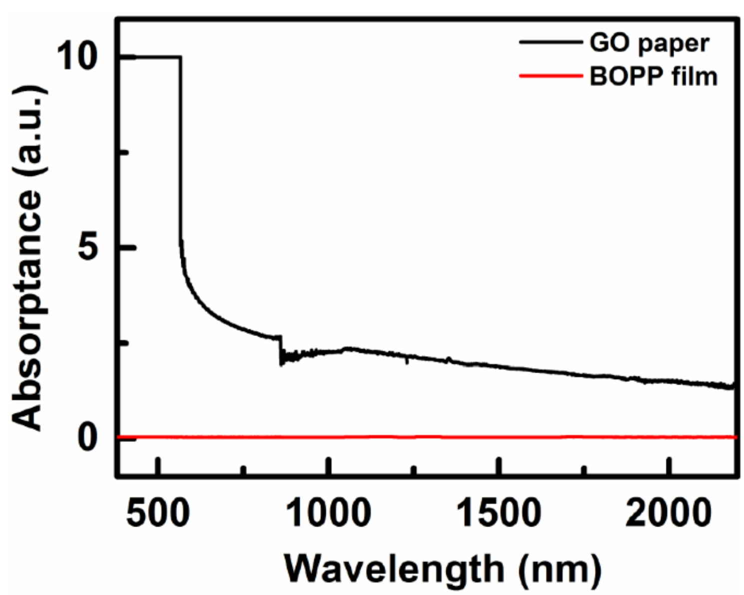

Fig. S10. Absorption spectrum of BOPP film and GO paper.

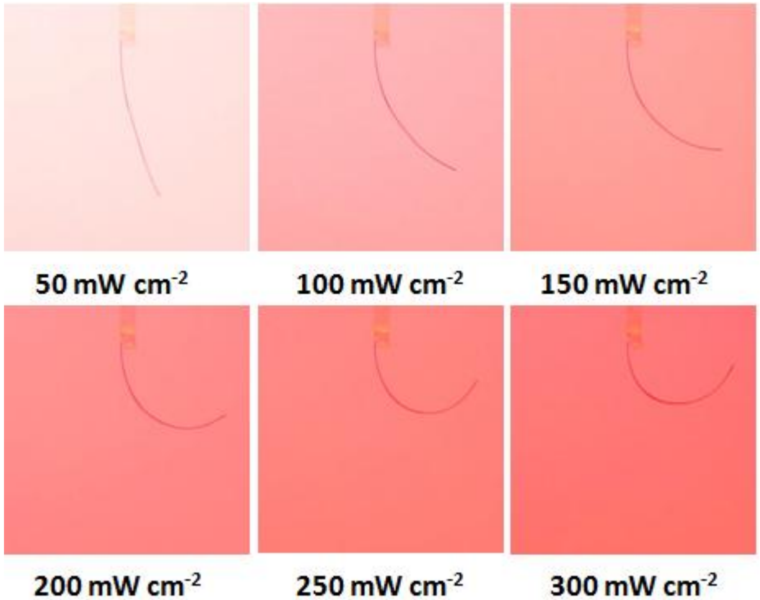

Fig. S11. Optical photos showing the actuation performances of the GO/BOPP actuator with different NIR light power densities for 10 s, respectively.

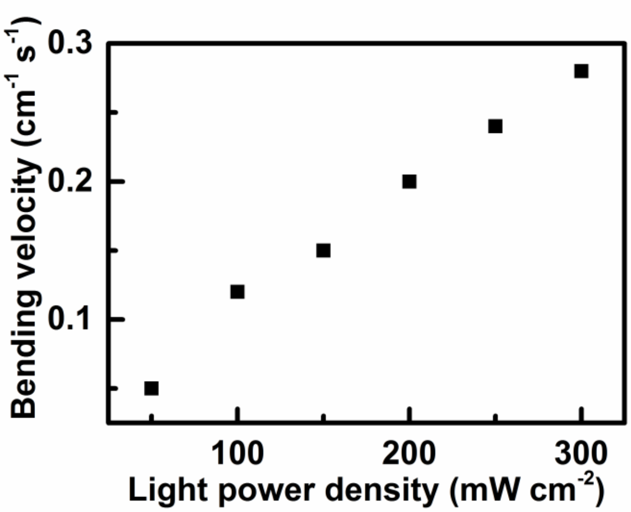

Fig. S12. Bending velocity of GO/BOPP actuator as a function of light power density. The NIR light power density is 300 mW cm^{-2}. The dimensions of the actuators are 15 mm × 2 mm × 65 μm (length × width × thickness).

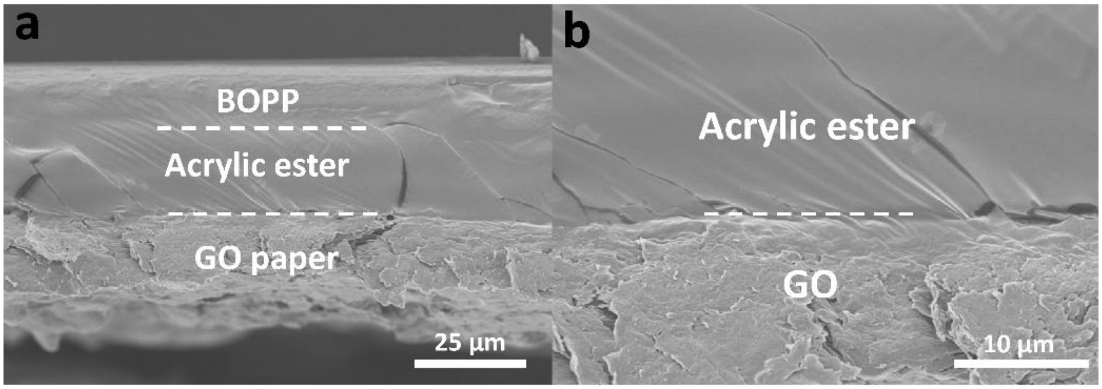

Fig. S13. Cross-sectional SEM images of the GO/BOPP actuator after repeatability test of NIR light-driven actuation.

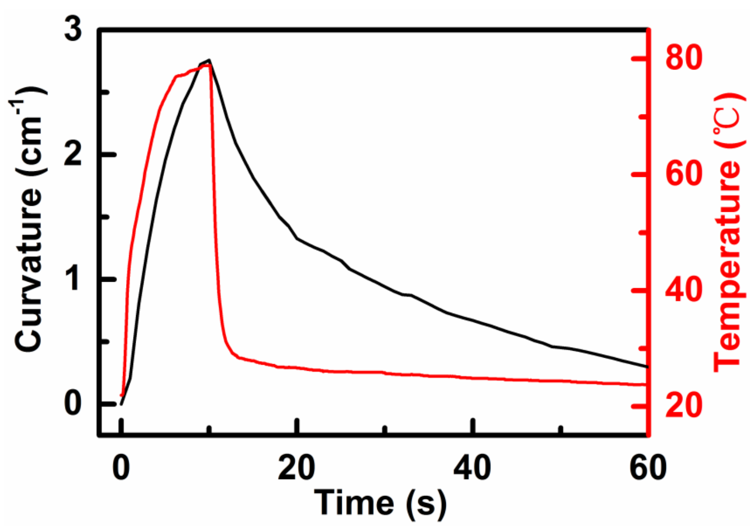

Fig. S14. Curvature (black line) and temperature (red line) of the GO/BOPP actuator as a function of time (RH = 50%). The NIR light power density is 300 mW cm^{-2}. The dimensions of the actuators are 15 mm × 2 mm × 65 μm (length × width × thickness).

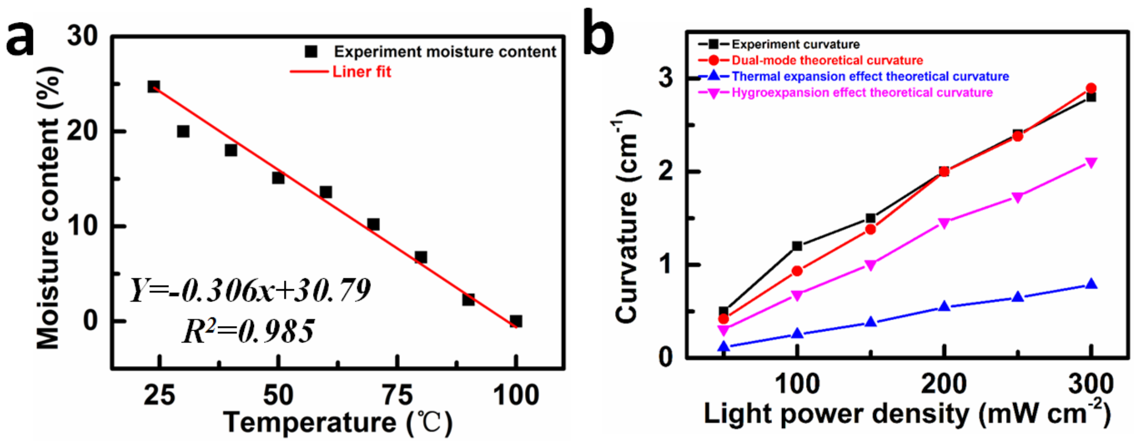

Fig. S15. (a) Moisture content of the GO paper as a function of temperature. (b) Expreimental curvature of GO/BOPP actuator (black square); theoretical curvature of GO/BOPP actuator based on the dual-mode actuation mechanism (red circle); theoretical curvature of GO/BOPP actuator considering only contraction of the GO paper (pink triangle); theoretical curvature of GO/BOPP actuator considering only thermal expansion of bilayers (blue triangle).

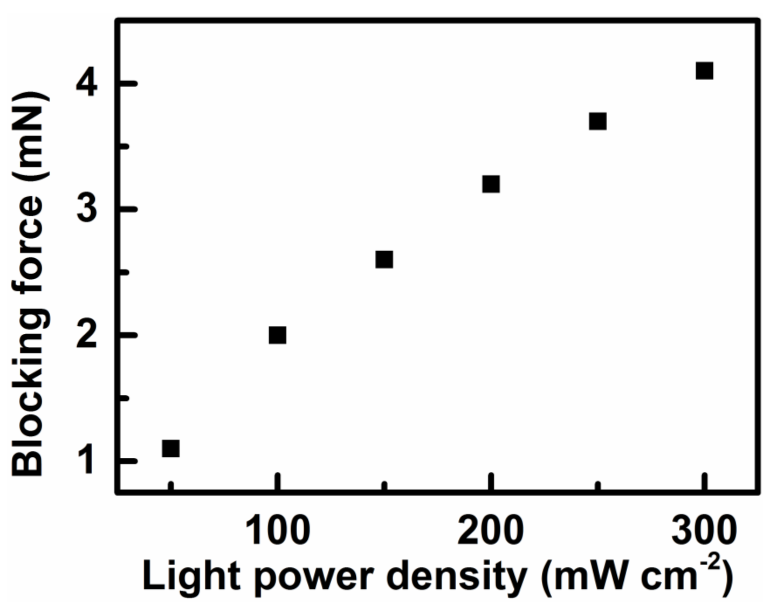

Fig. S16. Detected blocking force as a function of light power density.

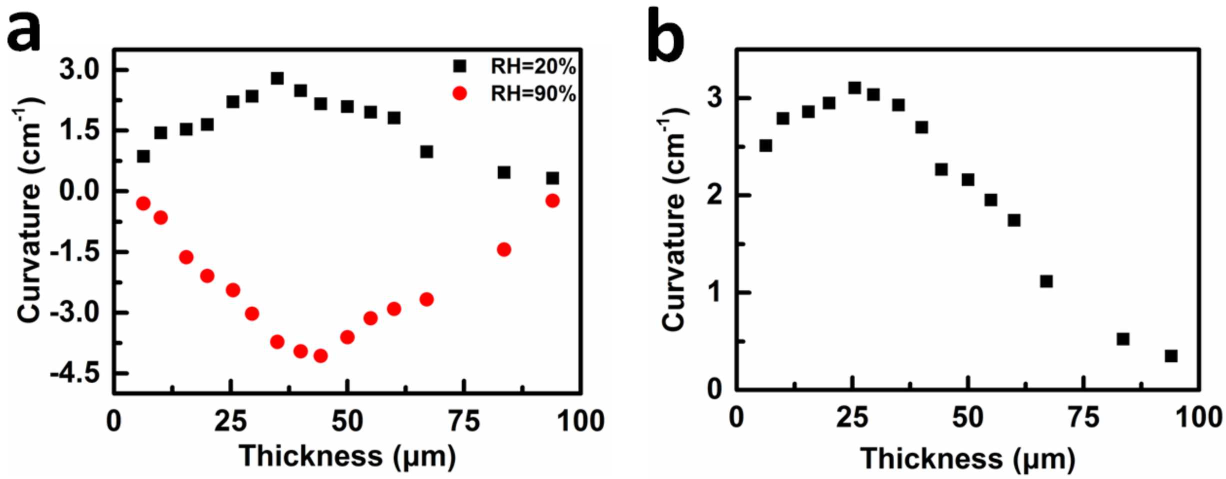

Fig. S17. The curvature of the GO/BOPP actuator as a function of GO layer thickness. (a) The actuators are driven by humidity changes (RH = 50% to RH = 20%; RH = 50% to RH = 90%). (b) The actuators are driven by NIR light (300 mW cm^{-2}).

Supplementary Tables

Table S1. Important physical parameters of some materials in flexible electronics.

	Materials	**Young's Modulus [Gpa]**	**CTE [ppm K^{-1}]**	**CHE [%RH^{-1}]**
Hygroscopic materials	**Paper**[5]	2-6	4-16	$3\text{-}19\times10^{-4}$
	PEDOT:PSS[6]	1.8-2.3	Not given	4.7×10^{-4}
	GO[4, 7, 8]	13-44	0.85 (intrinsic)	$2.7\text{-}9\times10^{-2}$
Polymers	**BOPP**[1, 6, 9]	1.1	137	Moisture absorbance < 0.03%
	PET[5, 9]	2.55	38	$5\text{-}85\times10^{-6}$
	PI[6, 10]	2.5-8	28	Moisture absorbance < 0.68%
	PVDF[5]	8.3	127	2.2×10^{-13}
	PDMS[6]	$0.4\text{-}3.5\times10^{-3}$	266-310	Not given
	PDMS (Ecoflex)[6]	$6.9\text{-}8.3\times10^{-5}$	279-284	Not given

Table S2. A comparison of recent reported actuators based on BOPP (PP) and GO with our reported GO/BOPP actuator.

Materials	Shape	Driving method	Power density /Temperature	RH range [%]	Response time [s]	Max curvature [cm^{-1}] / Bending Angle [°]
GO/BOPP (This work)	**film**	**NIR light**	**300 [mW m^{-2}]**	**N/A**	**10**	**2.8 cm^{-1}**
		humidity	**N/A**	**20-90**	**60**	**3.1 cm^{-1}**
OD_H–$PDPA_{C1}$/BOPP[11]	film	Thermal	10 - 40 [℃]	N/A	Not given	2.5 cm^{-1}
BOPP/SACNT[2]	film	electrical	31 [mW cm^{-3}]	N/A	10	1.0 cm^{-1} (>360°)
BOPP/SACNT/PET[9]	film	electrical	14.3 [mW cm^{-3}]	N/A	30	0.41 cm^{-1}
BOPP/graphite/paper[1]	film	NIR light	300 mW cm^{-2}	N/A	10	1.9 cm^{-1}
		humidity	N/A	20-70	60	1.7 cm^{-1}
AgNWs-PEDOT:PSS/Paper/PP[6]	film	electrical	140 [mW cm^{-2}]	N/A	20	1.08 cm^{-1}
PDA-RGO/NOA-63[12]	film	812 nm NIR laser	22 [mW cm^{-2}]	N/A	2	90°
		humidity	N/A	7-80	46	0.6 to 2 cm^{-1}
RGO–CNT/PDMS[13]	film	Simulated sunlight	250 [W cm^{-2}]	N/A	3.6	84° to 563°
GO-PDA/rGO[14]	film	NIR light	250 [mW cm^{-2}]	N/A	2	~180°
rGO/GO[15]	film	Simulated sunlight	150 [mW cm^{-2}]	N/A	0.73	~100°
G/GO[4]	fiber	humidity	N/A	10-80	Not given	-0.5 to 2.4 cm^{-1}
GO/RGO[16]	film	humidity	N/A	24-86	15	0 to 2.4 cm^{-1}
GO/RGO[17]	film	humidity	N/A	24-97	5	0 to 1.7 cm^{-1}
GO/prGO-PPy[18]	film	humidity	N/A	6.5-65	Not given	330°
GO/rGO[19]	film	humidity	N/A	0-85	Not given	<120°

Supplementary references:

1 M. Weng, P. Zhou, L. Chen, L. Zhang, W. Zhang, Z. Huang, C. Liu and S. Fan, *Adv. Funct. Mater.*, 2016, **26**, 7244.

2 L. Chen, M. Weng, Z. Zhou, Y. Zhou, L. Zhang, J. Li, Z. Huang, W. Zhang, C. Liu and S. Fan, *ACS Nano*, 2015, **9**, 12189.

3 S. Timoshenko, *J. Opt. Soc. Am.*, 1925, **11**, 233.

4 H. Cheng, J. Liu, Y. Zhao, C. Hu, Z. Zhang, N. Chen, L. Jiang and L. Qu, *Angew. Chem. Int. Ed.*, 2013, **52**, 10482.

5 Y. Tai, G. Lubineau and Z. Yang, *Adv. Mater.*, 2016, **28**, 4665.

6 M. Amjadi and M. Sitti, *ACS Nano*, 2016, **10**, 10202.

7 J. Zhu, C. M. Andres, J. Xu, A. Ramamoorthy, T. Tsotsis and N. A. Kotov, *ACS Nano*, 2012, **6**, 8357.

8 D. A. Dikin, S. Stankovich, E. J. Zimney, R. D. Piner, G. H. B. Dommett, G. Evmenenko, S. T. Nguyen and R. S. Ruoff, *Nature*, 2007, **448**, 457.

9 L. Chen, M. Weng, W. Zhang, Z. Zhou, Y. Zhou, D. Xia, J. Li, Z. Huang, C. Liu and S. Fan, *Nanoscale*, 2016, **8**, 6877.

10 J. Deng, J. Li, P. Chen, X. Fang, X. Sun, Y. Jiang, W. Weng, B. Wang and H. Peng, *J. Am. Chem. Soc.*, 2016, **138**, 225.

11 Y. Jin, B. Shin-Il Kim, W. Lee, C. Lee, H. Kim, K. Song, S. Jang and G. Kwak, *NPG Asia Mater.*, 2014, **6**, e137.

12 M. Ji, N. Jiang, J. Chang and J. Sun, *Adv. Funct. Mater.*, 2014, **24**, 5412.

13 Y. Hu, G. Wu, T. Lan, J. Zhao, Y. Liu and W. Chen, *Adv. Mater.*, 2015, **27**, 7867.

14 J. Mu, C. Hou, H. Wang, Y. Li, Q. Zhang and M. Zhu, *Sci. Adv.*, 2015, **1**, e1500533.

15 J. Mu, C. Hou, B. Zhu, H. Wang, Y. Li and Q. Zhang, *Sci. Rep.*, 2015, **5**, 9503.

16 D. Han, Y. Zhang, H. Jiang, H. Xia, J. Feng, Q. Chen, H. Xu and H. Sun, *Adv. Mater.*, 2015, **27**, 332.

17 D. Han, Y. Zhang, Y. Liu, Y. Liu, H. Jiang, B. Han, X. Fu, H. Ding, H. Xu and H. Sun, *Adv. Funct. Mater.*, 2015, **25**, 4548.

18 Y. Jiang, C. Hu, H. Cheng, C. Li, T. Xu, Y. Zhao, H. Shao and L. Qu, *ACS Nano*, 2016, **10**, 4735.

19 H. Cheng, F. Zhao, J. Xue, G. Shi, L. Jiang and L. Qu, *ACS Nano*, 2016, **10**, 9529.